Boulder School for Condensed Matter and Materials Physics

Laurette Tuckerman

laurette@pmmh.espci.fr

Pattern Formation:

Swift-Hohenberg, Ginzburg-Landau, Newell-Whitehead Segur equations

Stripes, travelling and standing waves, squares and hexagons

Busse balloon, Eckhaus and zig-zag instability

Sources:

R. Hoyle, Pattern Formation: An Introduction to Methods, Cambridge 2006

M. Cross, http://www.its.caltech.edu/∼ mcc

1 Pattern formation

On a domain which is not constrained by horizontal boundary conditions, i.e. which is horizontally homogeneous, the eigenvectors responsible for pattern formation are necessarily of the form $\exp(i\boldsymbol{q}\cdot\boldsymbol{x})$ where we take $\boldsymbol{x} = (x, y)$. The linear instability depends only on the wavenumber q and not on its direction $\boldsymbol{q}$. From the simple pitchfork bifurcation normal form $\dot{A} = \mu A - A^3$ we are familiar with the idea that the nonlinear term determines the magnitude of the final state, e.g. $A = \pm\sqrt{\mu}$ for the pitchfork. In addition, though, when there are multiple bifurcating eigenvectors – corresponding to different directions of $\boldsymbol{q}$ – the nonlinear terms will determine the pattern via the relative magnitudes of the eigenvectors with different orientations of $\boldsymbol{q}$.

The fact that the eigenspace is not merely multi-dimensional but infinite dimensional (all possible orientations of $\boldsymbol{q}$) leads to mathematical difficulties that are not yet resolved. The current theoretical framework calls for restricting the eigenvectors to a finite set by setting the problem on a specified lattice. Thus, we seek solutions with a fixed pattern – stripes, rectangles, squares, hexagons – and determine the properties of these solutions, but we do not address the complete problem of determining the pattern.

1.1 Swift-Hohenberg equation

The **Swift-Hohenberg** (SH) equation was formulated by Swift and Hohenberg in 1977 as a model for the horizontal structure of convection, but turns out to describe features common to pattern formation in many kinds of systems. We can begin to motivate this equation as follows. Consider a trivial state $u = 0$ which loses stability to perturbations of the form $u \sim e^{\sigma t}e^{\pm i\boldsymbol{q}\cdot\boldsymbol{x}}$. If the physical configuration is isotropic, then the growth rate σ must depend on the magnitude but not the orientation (which includes the sign) of $\boldsymbol{q}$. To be differentiable, it must be a function of q^2 rather than of $|q|$. In order for perturbations with infinitely large wavenumbers to be damped, σ must be negative for large q^2, and in order for some perturbations to grow and patterns to be formed, σ must be positive for some range of q^2. Then the growth rate is of the form:

$$\sigma(q) = a_0 + a_2 q^2 - q^4 \tag{1}$$

where we have set $a_4 = 1$ by scaling time. Setting $q_c^2 \equiv a_2/2$ and $\mu \equiv a_0 + q_c^4$, (1) can be rewritten as:

$$\sigma(q) = \mu - (q_c^2 - q^2)^2 \tag{2}$$

The curve $\sigma(q)$ resembles that in figure 1.

Substituting $\sigma \to \partial_t$ and $-q^2 \to \nabla^2$ in (2) leads to the partial differential equation

$$\partial_t u = \mu u - (q_c^2 + \nabla^2)^2 u \tag{3}$$

In order to halt the exponential growth due to linear instability, one must also include a nonlinear saturating term. The nonlinear term chosen for the Swift-Hohenberg equation is usually (but not always) $-u^3$. Thus, the SH equation is:

$$\partial_t u = \left[\mu - (q_c^2 + \nabla^2)^2\right] u - u^3 \tag{4}$$

When the nonlinearity includes a quadratic term, then **hexagons** can be obtained; see figure 2. Lifshitz and Petrich further modified the SH equation by including two different critical wavenumbers and were able to simulate **quasipatterns**; see figure 2.

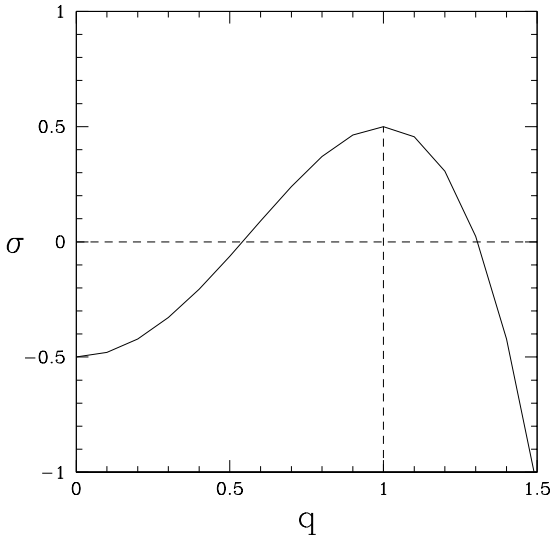

Figure 1: Growth rate σ as a function of spatial wavenumber q for the equation (4) with parameter values $q_c = 1$ and $\mu = 1/2$. The trivial $u = 0$ state is unstable to periodic perturbations with wavenumbers in an interval surrounding $q = q_c$.

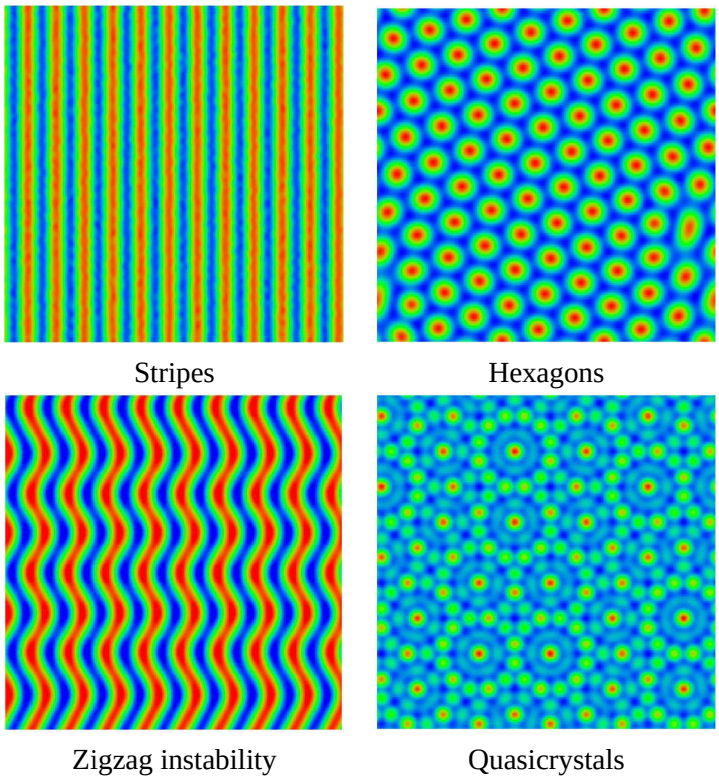

Figure 2: Patterns produced by Swift-Hohenberg equation and modifications of the SH equation. Simulations from Java applets of M. Cross, Caltech, `http://crossgroup.caltech.edu/Patterns`.

1.2 Stripes or Rolls

In the simplest case, we assume that the pattern depends only on one direction, x. Substituting $e^{\sigma t+iqx}$ into (4) and keeping only linear terms leads to

$$\sigma = \left[\mu - (q_c^2 - q^2)^2\right] \tag{5}$$

There are steady bifurcations ($\sigma = 0$) at

$$\mu_q = (q_c^2 - q^2)^2 \tag{6}$$

The *marginal stability curve* corresponding to (6) is shown in figure 3 (left).

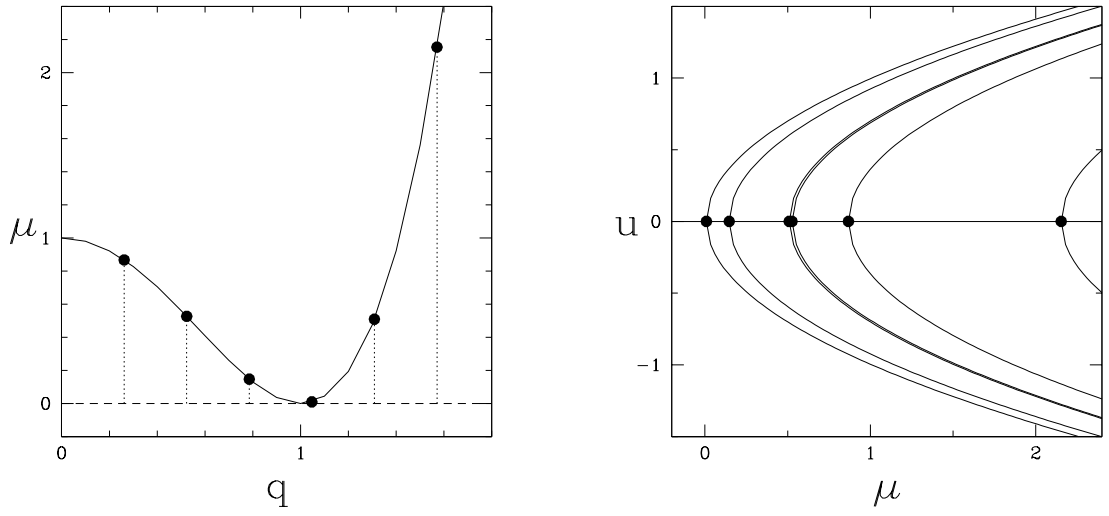

Figure 3: Swift-Hohenberg equation with $q_c = 1$. Left: Marginal curve. Dots indicate bifurcation points in periodic domain of width $L = 24$. Right: Schematic diagram of bifurcating branches for $L = 24$.

Imposing periodic boundary conditions in x with wavelength L restricts the allowed wavenumbers to the discrete set of multiples of $2\pi/L$

$$q = \frac{2\pi}{L}, \frac{4\pi}{L}, \frac{6\pi}{L}, \dots \tag{7}$$

The bifurcation with lowest μ occurs for the allowed value of q which is closest to q_c. In the Rayleigh-Bénard convection problem, the length scale was chosen as depth; in these units, $q_c = \pi/\sqrt{2} = 2.22$, $\lambda_c = \sqrt{2} = 1.4$ for free-slip bounding plates and $q_c = \pi = 3.14$, $\lambda_c = 2$ for rigid plates. For the Swift-Hohenberg equation, it is usual to choose a length scale for x such that $q_c = 1$, $\lambda_c = 2\pi$.

Figure 3 (right) shows the bifurcations and solutions emanating from them. The bifurcations here are all circle pitchforks, because any phase in x is permitted by the periodic boundary conditions. If the horizontal boundary conditions were Neumann boundary conditions ($\partial_x u|_{0,\pi} = 0$), the bifurcations would be ordinary pitchforks, with only two branches.

As q deviates from q_c, the bifurcation thresholds μ become larger: stripes with wavenumber q_c are favored and those with wavenumbers very different from q_c require more extreme conditions, here μ

very large. In a much smaller container, for example $L = \lambda_c = 2\pi$, the lowest bifurcation thresholds permitted after $\mu = 0$ would be $\mu = 9$ for $\lambda = L/2$ and $\mu = 64$ for $\lambda = L/3$. This limit is useful because bifurcations other than the first one are far away and can safely be neglected. In very large container, the bifurcation thresholds are very close together and the discretization is usually neglected.

In what follows we will study domains of varying sizes, ranging from a single critical wavelength through several wavelengths to an infinite number. In the remainder of this section, we will use the symmetry approach, rather than the Swift-Hohenberg equation, to study square and hexagonal patterns. Afterwards, we will study the instabilities of roll pattern by using the Newell-Whitehead-Segur equation, which is derived from the Swift-Hohenberg equation.

1.3 Travelling waves and standing waves

We first consider a Hopf bifurcation taking place on a periodic domain. This situation leads to traveling and standing waves and is described by a four-dimensional normal form. We use vectors (z_+, z_-) in which z_+ is the complex amplitude (representing the amplitude and phase) of left-going traveling waves and z_- is that of right-going traveling waves. The functional form of the fields is

$$u(\theta, t) = (z_+(t) + z_-(t))e^{i\theta} + (\bar{z}_+(t) + \bar{z}_-(t))e^{-i\theta} \tag{8}$$

At linear order, the evolution of $z_\pm(t)$ is described by

$$\frac{d}{dt}\begin{pmatrix} z_+ \\ z_- \end{pmatrix} = \begin{pmatrix} i\omega z_+ \\ -i\omega z_- \end{pmatrix} \tag{9}$$

so that the evolution to linear order is

$$u(\theta, t) = z_+(0)e^{i(\theta+\omega t)} + z_-(0)e^{i(\theta-\omega t)} + \bar{z}_+(0)e^{-i(\theta+\omega t)} + \bar{z}_-(0)e^{-i(\theta-\omega t)} \tag{10}$$

with $z_\pm(0)$ arbitrary initial amplitudes. Without justification, we give the simplest cubic order system of evolution equations:

$$\frac{d}{dt}\begin{pmatrix} z_+ \\ z_- \end{pmatrix} = \begin{pmatrix} (\mu + i\omega + a|z_-|^2 + b(|z_+|^2 + |z_-|^2)z_+ \\ (\mu - i\omega + \bar{a}|z_+|^2 + \bar{b}(|z_+|^2 + |z_-|^2)z_- \end{pmatrix} \tag{11}$$

Defining $z_\pm = r_\pm e^{i\phi_\pm}$ and $A^2 = r_+^2 + r_-^2$, from (11) we derive:

$$\frac{dr_\pm}{dt} = (\mu + a_r r_\mp^2 + b_r(r_+^2 + r_-^2))r_\pm \tag{12a}$$

$$\frac{d\phi_\pm}{dt} = \pm(\omega + a_i r_\mp^2 + b_i(r_+^2 + r_-^2)) \tag{12b}$$

Note that the equations (11) are independent of the phases $\phi_\pm$.
The solutions for which $dr_\pm/dt = 0$ are:

$$\text{the origin :} \quad r_+ = 0,\ r_- = 0 \tag{13a}$$

$$\text{the left traveling waves :} \quad r_+ = \sqrt{-\mu/b_r},\ r_- = 0, \quad \dot{\phi}_+ = \omega - \mu b_i/b_r \tag{13b}$$

$$\text{the right traveling waves :} \quad r_+ = 0,\ r_- = \sqrt{-\mu/b_r}, \quad \dot{\phi}_- = -(\omega - \mu b_i/b_r) \tag{13c}$$

$$\text{the standing waves :} \quad r_+ = r_- = \sqrt{-\mu/(a_r + 2b_r)}, \quad \dot{\phi}_\pm = \pm(\omega - \mu(a_i + 2b_i)/(a_r + 2b_r)) \tag{13d}$$

Standing and travelling waves are illustrated for a simulation of Rayleigh-Bénard convection in a cylindrical container in figures 4 and 5. Standing and travelling waves are illustrated for 2D simulations of thermosolutal convection in figure 6.

According to the signs and magnitudes of a and b, the standing waves and traveling waves branch in the same or the opposite directions in μ. If $b_r < 0$ (> 0), then the travelling waves exist for $\mu > 0$ (< 0) If $a_r + 2b_r < 0$ (< 0), then the standing waves exist for $\mu > 0$ (< 0). The lines $b_r = 0$ and $a_r + 2b_r = 0$ thus divide the (a_r, b_r) plane into four sections, as shown in figure 7.

The stability of these states is calculated as follows. At the origin, since angles are not defined, we must write the Jacobian in its Cartesian representation. We will not do this here and just state that at the origin, the Jacobian is μ times the identity and hence has four eigenvalues which change sign at μ, along with a four-dimensional eigenspace.

For the non-zero states, we can write the Jacobian in the polar $(r_+, r_-, \phi_+, \phi_-)$ coordinates:

$$\begin{pmatrix} \mu + a_r r_-^2 + b_r(r_+^2 + r_-^2) + 2b_r r_+^2 & 2(a_r + b_r) r_- r_+ & 0 & 0 \\ 2(a_r + b_r) r_- r_+ & \mu + a_r r_+^2 + b_r(r_+^2 + r_-^2) + 2b_r r_-^2 & 0 & 0 \\ 2b_i r_+ & 2(a_i + b_i) r_- & 0 & 0 \\ -2(a_i + b_i) r_+ & -2b_i r_+ & 0 & 0 \end{pmatrix} \tag{14}$$

Since (14) is block lower-triangular, its eigenvalues and eigenvectors are those of its diagonal blocks, as shown by:

$$\begin{pmatrix} A & 0 \\ C & D \end{pmatrix} \begin{pmatrix} X \\ Y \end{pmatrix} = \lambda \begin{pmatrix} X \\ Y \end{pmatrix} \tag{15}$$

$$\left.\begin{aligned} AX &= \lambda X \\ CX + DY &= \lambda Y \end{aligned}\right\} \Longrightarrow \left\{\begin{array}{l} X = 0 \\ (\lambda, Y) \text{ is an eigenpair of } D \end{array}\right\} \text{ or } \left\{\begin{array}{l} (\lambda, X) \text{ is an eigenpair of } A \\ Y = (\lambda I - D)^{-1} C X \end{array}\right\}$$

The eigenvalues of the $r_\pm$ direction are obtained via the formula for a general 2×2 matrix $\begin{pmatrix} \alpha & \beta \\ \gamma & \delta \end{pmatrix}$:

$$\lambda_\pm = \frac{\alpha + \delta}{2} \pm \sqrt{\left(\frac{\alpha - \delta}{2}\right)^2 + \beta\gamma} \tag{16}$$

Substituting the elements of (14) and the solutions (13) into (16) leads to

the origin :	μ along r_+	μ along r_-
the left traveling waves :	-2μ along r_+	$-a_r\mu/b_r$ along r_-
the right traveling waves :	-2μ along r_-	$-a_r\mu/b_r$ along r_+
the standing waves :	-2μ along (r_+, r_-)	$2a_r\mu/(a_r + 2b_r)$ perpendicular to (r_+, r_-)

If $b_r < 0$, then the travelling waves exist for $\mu > 0$, as shown in (13). Since $-2\mu < 0$, they are stable if and only if $a_r/b_r > 0$, i.e. in the lower left quadrant of the (a_r, b_r) plane, as shown in figure 7. If $b_r > 0$, then the travelling waves exist for $\mu < 0$, so $-2\mu > 0$ and they are not stable. Similarly, if $a_r + 2b_r < 0$, then the standing waves exist for $\mu > 0$ and they are stable if $a_r > 0$, i.e. in the upper-left wedge of the (a_r, b_r) plane. If $a_r + 2b_r > 0$, then the standing waves exist for $\mu < 0$ and so $-2\mu > 0$ and they are not stable.

Some general conclusions are that either the standing waves or the traveling waves are stable, or neither are stable. If one solution is stable, it is that which has the largest amplitude $\sqrt{r_+^2 + r_-^2}$. If neither are stable, then $r_\pm \to \infty$ for some choices of initial conditions or μ-values, unless higher order terms are added to (12a) or (11). This is shown in figures 7 and 8.

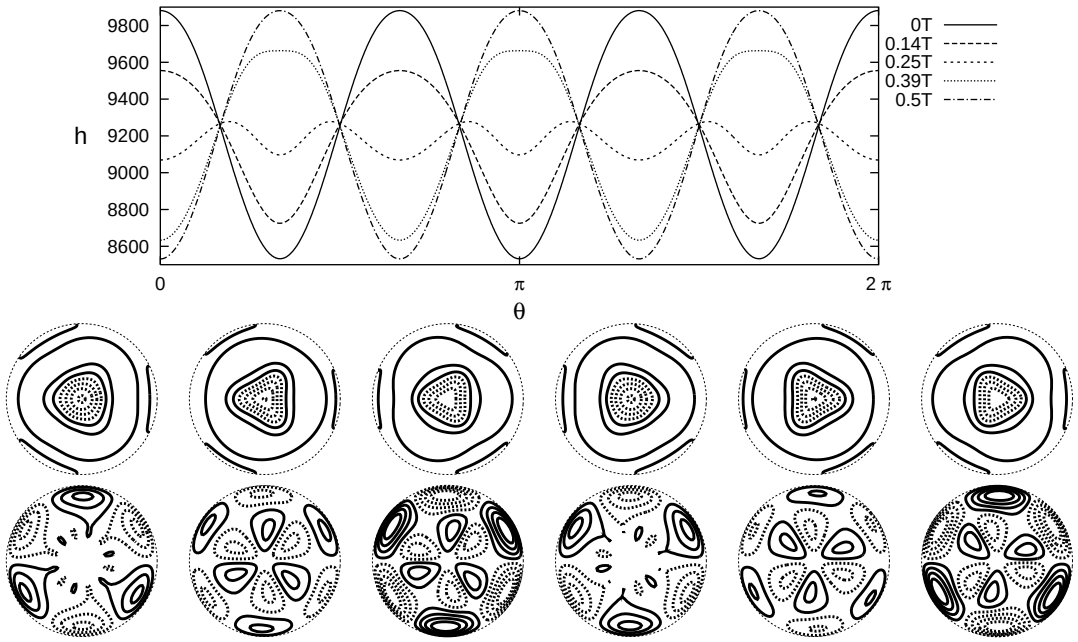

Figure 4: Standing waves in Rayleigh-Bénard convection in a cylinder with $\Gamma = R/H = 1.47$ and $Pr = 1$ at at $Ra = 26\,000$. Top row: temperature versus θ at $(r, z) = (0.7, 0.3)$ at five successive times during one oscillation period T. Middle and bottom rows: contours of temperature (middle) and of azimuthal velocity (bottom) on the midplane at $t = 0$, $T/6$, $2T/6$, $3T/6$, $4T/6$, $5T/6$. From Borońska & Tuckerman, J. Fluid Mech. **559**, 279 (2006).

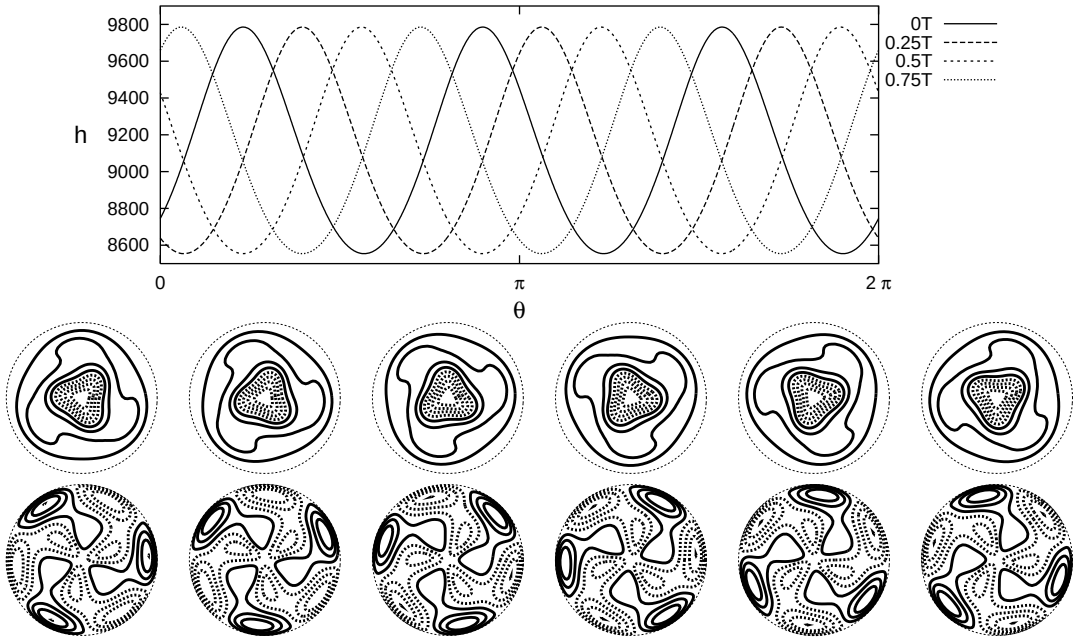

Figure 5: Counterclockwise travelling wave in Rayleigh-Bénard convection in a cylinder with $\Gamma = R/H = 1.47$ and $Pr = 1$ at $Ra = 26\,000$. Top row: temperature versus angle θ for $(r, z) = (0.7, 0.3)$, at four different instants during one oscillation period T. Middle and bottom rows: contours of temperature (middle) and of azimuthal velocity (bottom) on the midplane at $t = 0$, $T/6$, $2T/6$, $3T/6$, $4T/6$, $5T/6$. From Borońska & Tuckerman, J. Fluid Mech. **559**, 279 (2006).

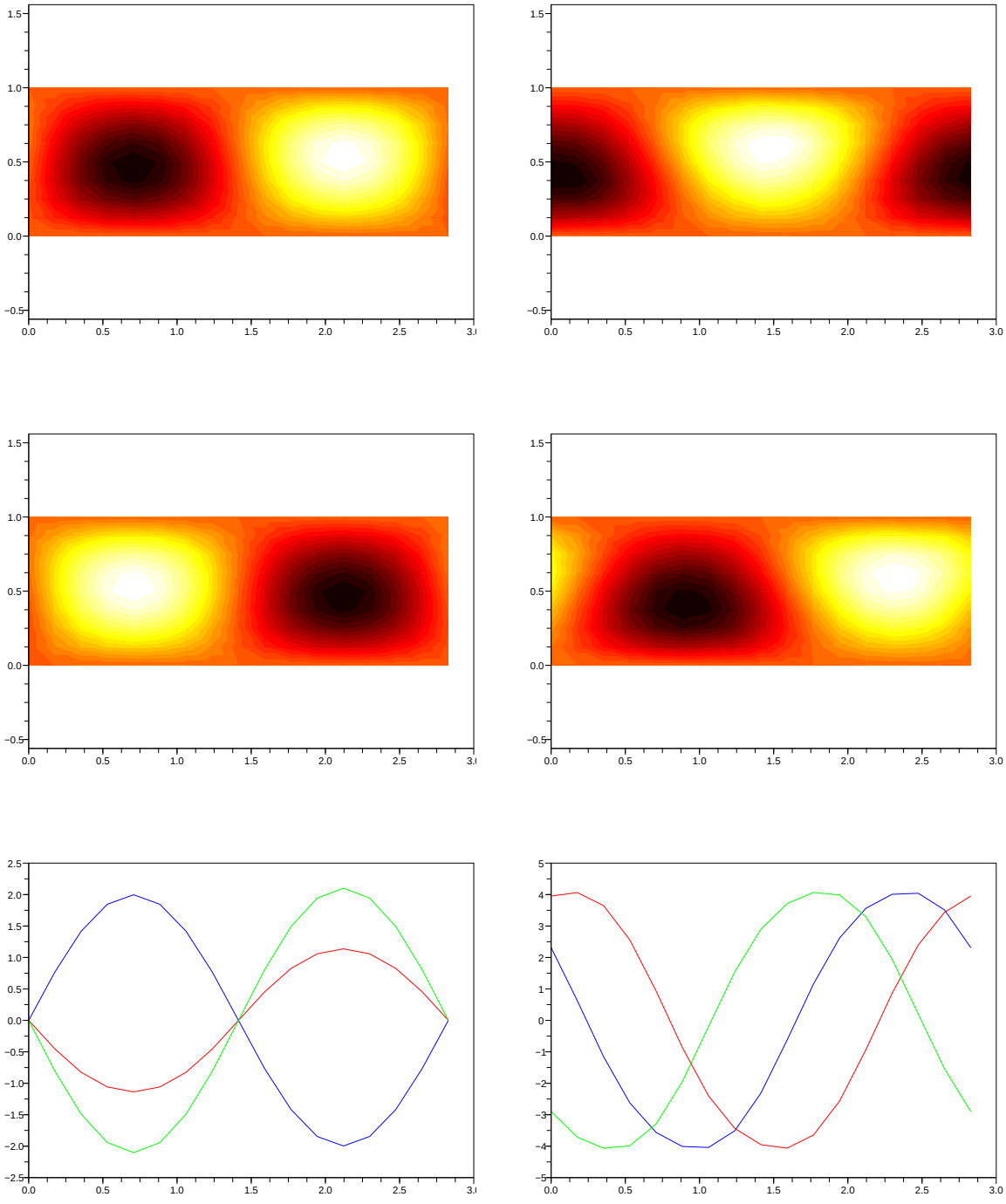

Figure 6: Simulation of 2D thermosolutal convection with horizontally periodic and vertical free-slip boundary conditions. Parameters are $S = -0.1$, $L = 0.1$, $Pr = 10$, and $r \equiv Ra/Ra_c = 1.3$. Above: temperature field at two successive times. Below: wave profiles at mid-height at successive times. Left: standing waves. Right: travelling waves.

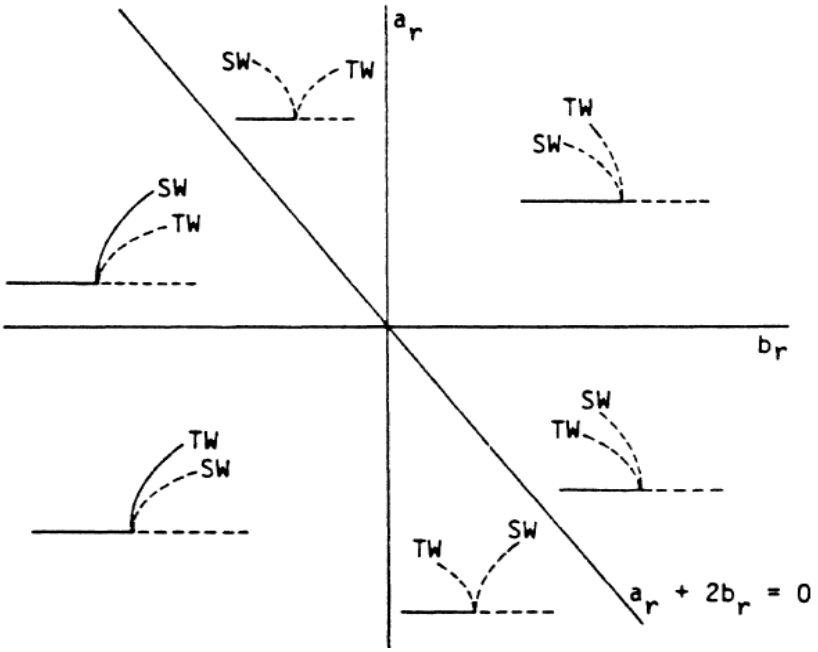

Figure 7: Stability and branching direction of standing waves (SW) and travelling waves (TW) in the parameter plane of the nonlinear coefficients (a_r, b_r). From Knobloch, Phys. Rev. A **34**, 1538 (1986).

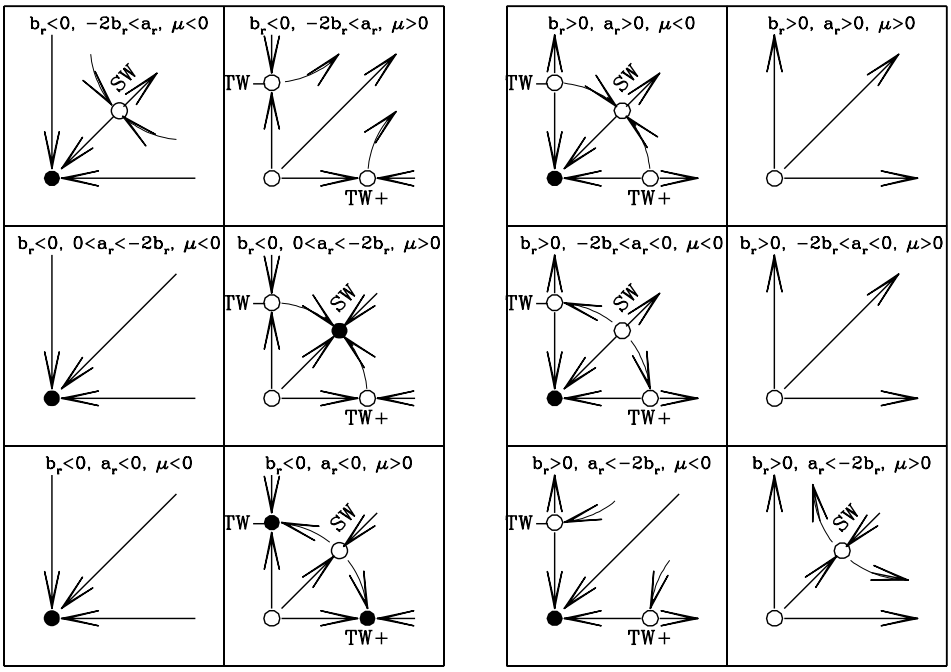

Figure 8: Phase diagrams for Hopf bifurcation in periodic domain. Each diagram shows (r_+, r_-) plane.

1.4 Square patterns

We now consider steady patterns that vary in two directions, x_1 and x_2. We impose periodicity length $L = \lambda_c = 2\pi$ in both of these directions, so that the domain is a periodically repeating square. The eigenvectors are then $e^{\pm ix_1}$ and $e^{\pm ix_2}$. We write nonlinear solutions as

$$u(x_1, x_2, t) = z_1(t)e^{ix_1} + \bar{z}_1(t)e^{-ix_1} + z_2(t)e^{ix_2} + \bar{z}_2(t)e^{-ix_2} \tag{17}$$

The appropriate equations governing the evolution of the amplitudes $z_1(t)$ and $z_2(t)$ turn out to be:

$$\dot{z}_1 = \mu z_1 - (a|z_1|^2 + b|z_2|^2)z_1 \tag{18a}$$
$$\dot{z}_2 = \mu z_2 - (b|z_1|^2 + a|z_2|^2)z_2 \tag{18b}$$

The reasoning behind the form of these equations is that:
–The x_1 and x_2 directions are equivalent. Hence the linear coefficient μ, the self-saturation coefficient a, and the cross-saturation coefficient are the same in both equations. –The allowed nonlinear terms are dictated by the fact that
$e^{ix_1}e^{-ix_1}e^{ix_1} = e^{ix_2}e^{-ix_2}e^{ix_1} = e^{ix_1}$ and $e^{ix_1}e^{-ix_1}e^{ix_2} = e^{ix_2}e^{-ix_2}e^{ix_2} = e^{ix_2}$. The spatial phases can be eliminated by shifting the origin, so we can replace the complex z_1, z_2 by real r_1, r_2. The solutions are:

–Rolls in the x_1 direction ($r_1 \neq 0$, $r_2 = 0$) or in the x_2 direction ($r_1 = 0$, $r_2 \neq 0$)
–Squares with $r_1 = r_2$

Depending on the nonlinear coefficients a, b, the rolls and squares can branch in the same direction or in opposite directions. If they branch in opposite directions, rolls and squares are both unstable. If they both branch in the direction of increasing eigenvalue μ, either rolls or squares are stable. If they both branch in the direction of decreasing eigenvalue μ, then neither are stable. We will demonstrate this in the next section.

Squares are an equal superposition of rolls in the x_1 and x_2 directions. Choosing the origin such that $z_1 = z_2 = r$, equation (17) reduces to

$$\begin{aligned} u(x_1, x_2, t) &= z_1(t)e^{ix_1} + z_2(t)e^{ix_2} + \bar{z}_1(t)e^{-ix_1} + \bar{z}_2(t)e^{-ix_2} \\ &= r(t)e^{ix_1} + r(t)e^{ix_2} + r(t)e^{-ix_1} + r(t)e^{-ix_2} \\ &= 2r(t)(\cos(x_1) + \cos(x_2)) \\ &= 4r(t)\cos\left(\frac{x_1 + x_2}{2}\right)\cos\left(\frac{x_1 - x_2}{2}\right) \end{aligned} \tag{19}$$

We see from (19) that the nodal lines $u = 0$ are

$$x_1 + x_2 = \pi + 2n\pi, \qquad x_1 - x_2 = \pi + 2n\pi \tag{20}$$

i.e. diagonals with slopes ± 1, as in figure 9.

These properties also hold for patterns in a finite square box. An eigenvector consisting of a pair of rolls can be rotated by $\pi/2$ so that the rolls are oriented in the x_1 or the x_2 direction. Any linear combination of these eigenvectors is also an eigenvector. However, the nonlinear terms restrict the set of permitted patterns to four: x_1 rolls and x_2 rolls, and $+$ and $-$ diagonals. When the featureless state loses stability to this set of eigenvectors, four branches are necessarily created. The roll solutions are obtained from one another by rotation symmetry and thus necessarily dynamically equivalent to one another; for example,

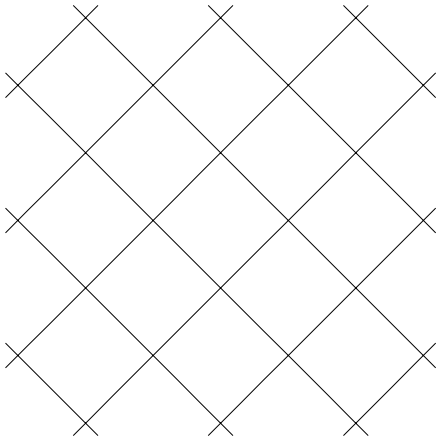

Figure 9: Nodal lines of square pattern.

both will undergo the same secondary bifurcations. Similarly, the two diagonal solutions are dynamically equivalent to one another. But the roll and diagonal solutions are not equivalent to one another and will usually have different secondary bifurcations.

This is illustrated in a simulation of Marangoni convection in a 3D box with equal dimensions in x and y, shown in figures 10 and 11. Like Rayleigh-Bénard convection, Marangoni convection consists of fluid motion arising from thermal gradients, but in Marangoni convection, it is the temperature dependence of the surface tension at a free surface which is reponsible, rather than the temperature dependence of the density. The pitchfork bifurcation P_1 from the trivial state creates four branches of convective states. Although the straight and diagonal states have different stability properties and so undergo different secondary bifurcations, they all disappear simultaneously for the same reason that they are created simultaneously. Other bifurcations occur to eigenvectors with different symmetries. In particular, bifurcation T_1, to an eigenvector with the same symmetry as the square box, is a transcritical bifurcation.

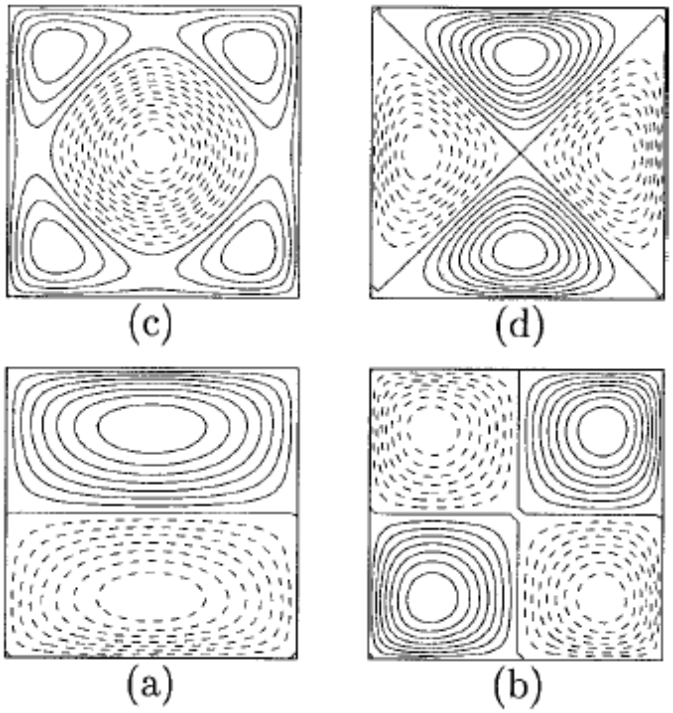

FIG. 2. Critical vertical velocity eigenfunctions at the primary bifurcation points P_1, P_2, T_1, and P_3 for $A_x=A_y=1.5$ with (a) $\mathrm{Ma}_{P_1}=127.86$ ($\mathbf{Z}_2$-symmetric, fixed by $\mathcal{S}_x$), (b) $\mathrm{Ma}_{P_2}=204.3$ ($\mathbf{D}_2$-symmetric, fixed by Π_{xy} and Π_{yx}), (c) $\mathrm{Ma}_{T_1}=224.1$ ($\mathbf{D}_4$-symmetric, fixed by $\mathcal{S}_x$ and Π_{xy} and their products), and (d) $\mathrm{Ma}_{P_3}=248.6$ ($\mathbf{D}_2$-symmetric, fixed by $\mathcal{S}_x$ and $\mathcal{S}_y$). The symmetry of the eigenfunction (a) indicates that P_1 corresponds to a double zero eigenvalue: $\pi/2$ rotation of (a) about $x=y=0$ generates an independent eigenfunction. The resolution is $N_x\times N_y\times N_z=15\times 15\times 13$.

Figure 10: From Bergeon, Henry, Knobloch, *Three-dimensional Marangoni-Bénard flows in square and nearly square containers*, Physics of Fluids **13**, 92 (2001).

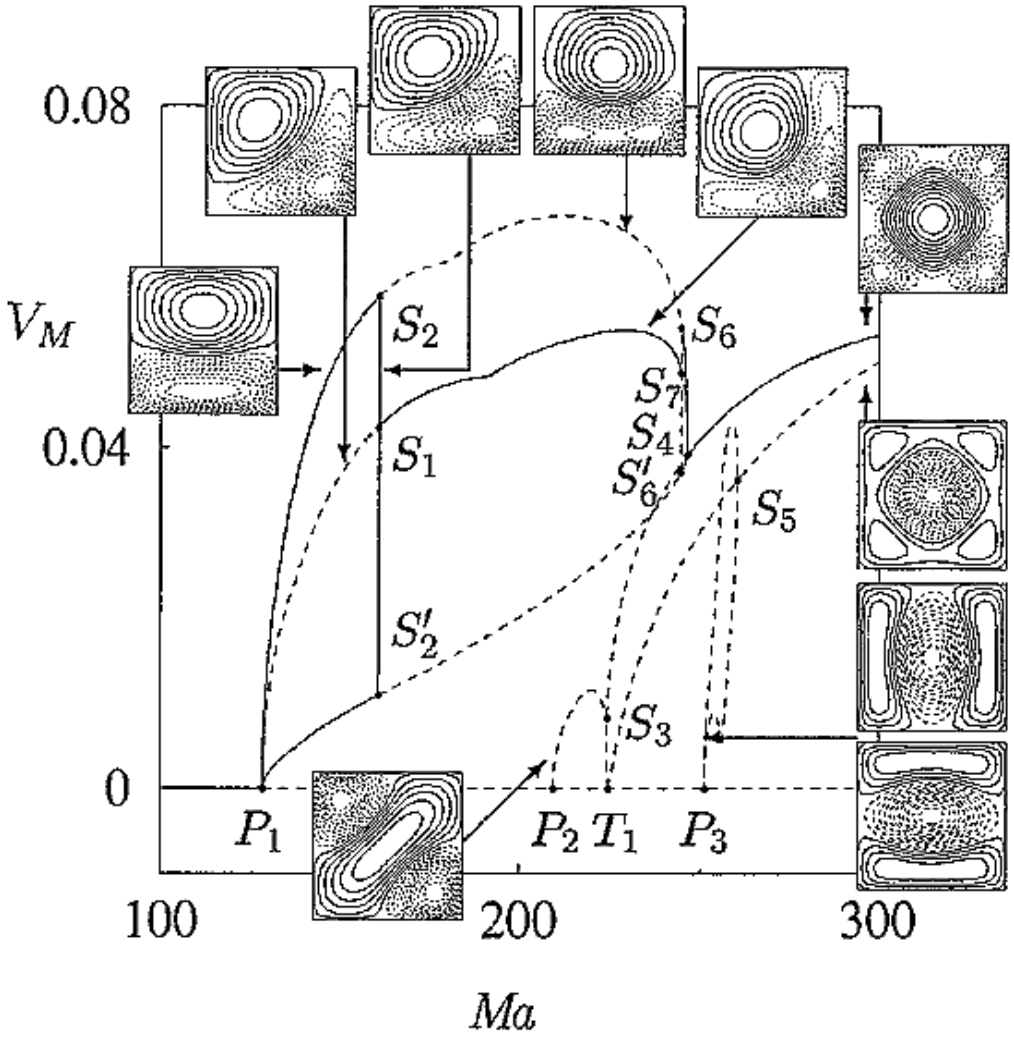

Figure 11: Simulation of Marangoni convection in a container with square horizontal cross section. From Bergeon, Henry, Knobloch, *Three-dimensional Marangoni-Bénard flows in square and nearly square containers*, Physics of Fluids **13**, 92 (2001).

1.5 Hexagons

We now consider a hexagonal lattice. We define three wavevectors $\boldsymbol{k}_j = (\cos 2\pi(j-1)/3, \sin 2\pi(j-1)/3)$ oriented at angles of 120° to one another, as in figure 12. We write solutions

$$u(x,y,t) = z_1(t)e^{i\boldsymbol{k}_1\cdot\boldsymbol{x}} + z_2(t)e^{i\boldsymbol{k}_2\cdot\boldsymbol{x}} + z_3(t)e^{i\boldsymbol{k}_3\cdot\boldsymbol{x}} + c.c. \tag{21}$$

and seek equations of evolution for (z_1, z_2, z_3).

It can be shown that, contrary to the square case, the governing equations in the hexagonal case contains quadratic terms, basically because $\boldsymbol{k}_1 + \boldsymbol{k}_2 + \boldsymbol{k}_3 = 0$. The resulting equations to cubic order are:

$$\dot{z}_1 = \left(\mu - b|z_1|^2 - c(|z_2|^2 + |z_3|^2)\right) z_1 + a\bar{z}_2\bar{z}_3 \tag{22}$$

and similarly for z_2, z_3, with real coefficients.

Hexagons are an equal superposition of three sets of rolls of equal amplitudes. Writing $z_j = r_j e^{i\phi_j}$, hexagonal solutions have $r_1 = r_2 = r_3 = r$. The evolution equation (22) for z_1 becomes

$$\dot{z}_1 = \left(\dot{r} + ri\dot{\phi}_1\right) e^{i\phi_1} = (\mu - (b+2c)r^2)re^{i\phi_1} + ar^2 e^{-i(\phi_2+\phi_3)} \tag{23}$$

and similarly for z_2, z_3. Dividing (23) by $e^{i\phi_1}$

$$\left(\dot{r} + ri\dot{\phi}_1\right) = (\mu - (b+2c)r^2)r + ar^2 e^{-i(\phi_1+\phi_2+\phi_3)} \tag{24}$$

and separating into real and imaginary parts leads to:

$$\dot{r} = (\mu - (b+2c)r^2)r + ar^2\cos(\phi_1+\phi_2+\phi_3) \tag{25a}$$

$$r\dot{\phi}_1 = ar^2\sin(\phi_1+\phi_2+\phi_3) \tag{25b}$$

and similarly for ϕ_2, ϕ_3.

Thus, steady states obey

$$\Phi \equiv \phi_1+\phi_2+\phi_3 = 0,\pi \implies \cos(\Phi) = \pm 1 \tag{26a}$$

$$0 = \mu - (b+2c)r^2 \pm ar \implies r = \begin{cases} \frac{1}{b+2c}\left[-a \pm \sqrt{a^2+4\mu(b+2c)}\right] \\ \frac{1}{b+2c}\left[+a \pm \sqrt{a^2+4\mu(b+2c)}\right] \end{cases} \tag{26b}$$

The meaning of $\Phi = \phi_1+\phi_2+\phi_3$ is as follows. Each of the three sets of rolls has a spatial phase ϕ_j. Two of these phases can be set to zero by shifting the origin. But the third phase relative to the other two cannot. The two possible values for Φ lead to hexagonal patterns that are not equivalent, called up-hexagons and down-hexagons, shown schematically in figure 13.

Equation (26b) would seem to represent four solutions, i.e. two parabolas, one symmetric about $r = -a$ and the other about $r = a$. However, requiring $r \geq 0$ reduces the four solutions to two. These solutions both bifurcate *transcritically* from the trivial state at $\mu = 0$. The turning point (saddle-node bifurcation) is at $\mu = -a^2/(4(b+2c))$, where $r = a$.

A number of non-trivial solution types exist in addition to hexagons: rolls, rectangles and triangles. The rolls are created in a pitchfork bifurcation and the rectangles in a secondary bifurcation from the roll branch. The trivial solution and up-hexagons are both stable over a range of μ, and the rolls and up-hexagons are also both stable over a different μ-interval. These are shown in the bifurcation diagram on the right portion of figure 12

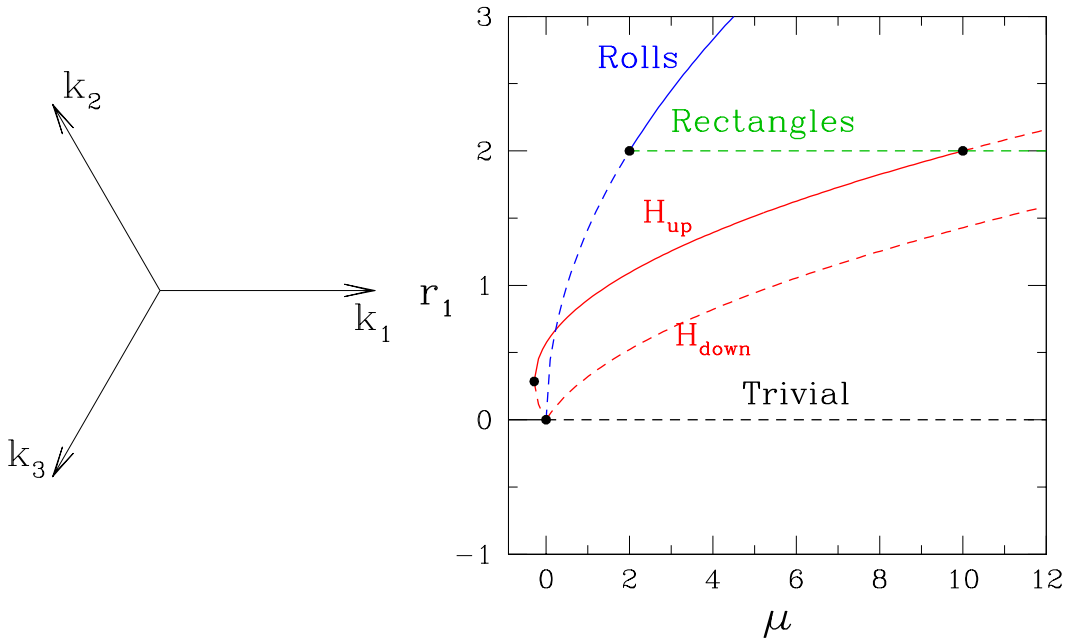

Figure 12: Left: wavevectors for hexagonal lattice. Right: Bifurcation diagram showing rolls (R), up-hexagons (H_{up}) and down-hexagons (H_{down}).

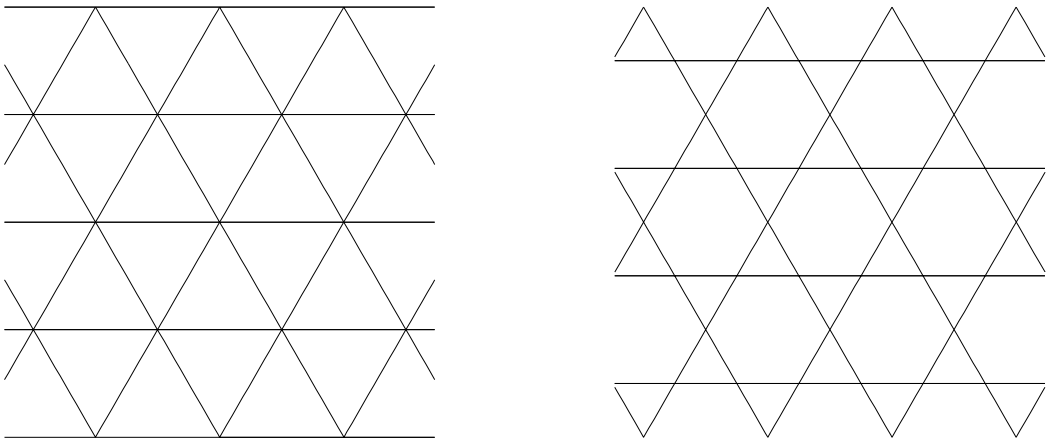

Figure 13: Hexagonal patterns. Left: up hexagons. Right: down hexagons.

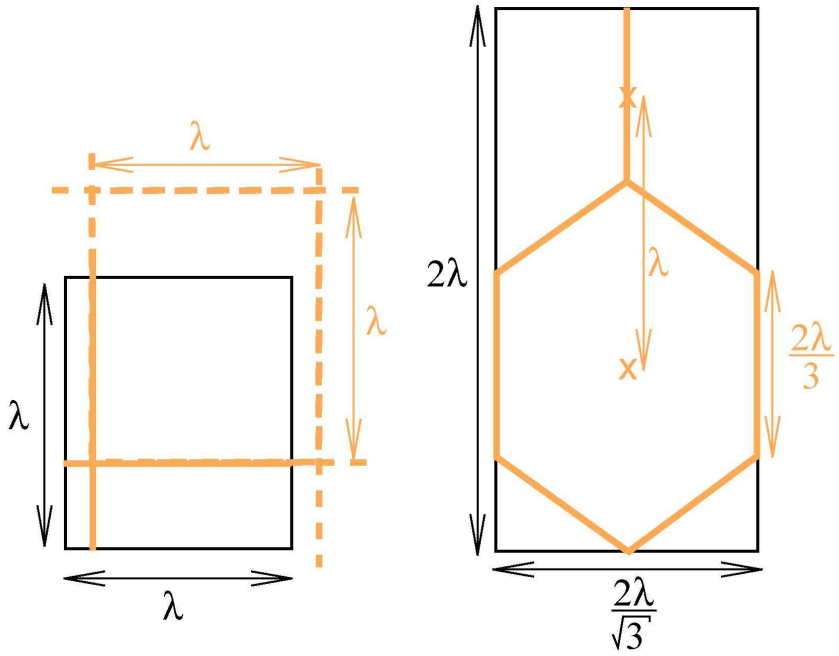

Figure 14: Boxes supporting the periodic patterns in the square and hexagonal cases. In black, the borders of the box. Bright lines, pattern contained by each box. $\lambda = 2\pi/k_c$.

1.6 Squares and hexagons in simulation of Faraday experiment

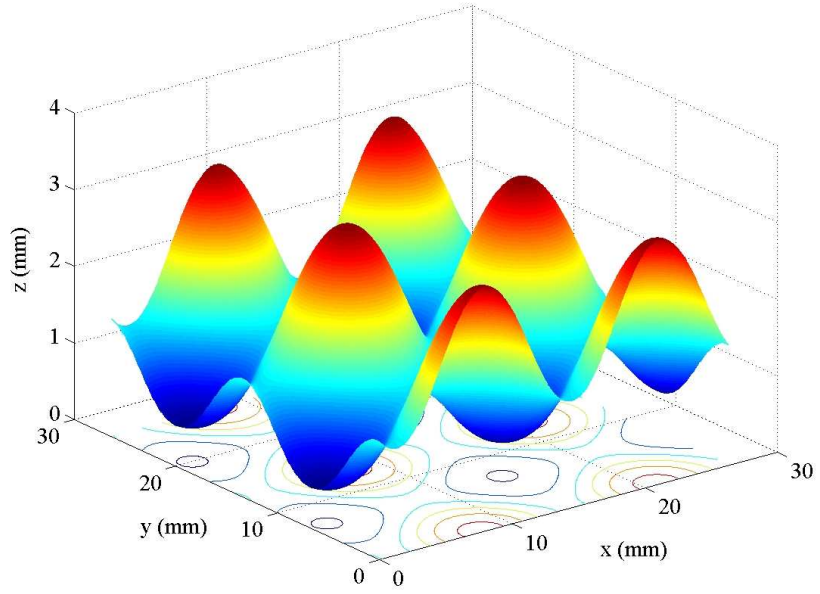
z (mm)
4
3
2
1
0
30
20
y (mm)
10
0
0
10
20
30
x (mm)

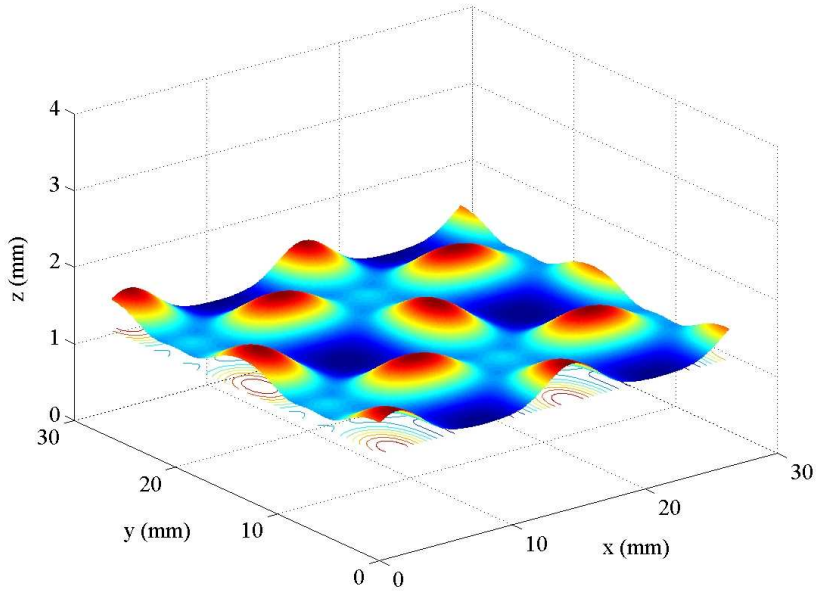
z (mm)
4
3
2
1
0
30
20
y (mm)
10
0
0
10
20
30
x (mm)

Hexagonal pattern: instantaneous position of interface and velocity fields

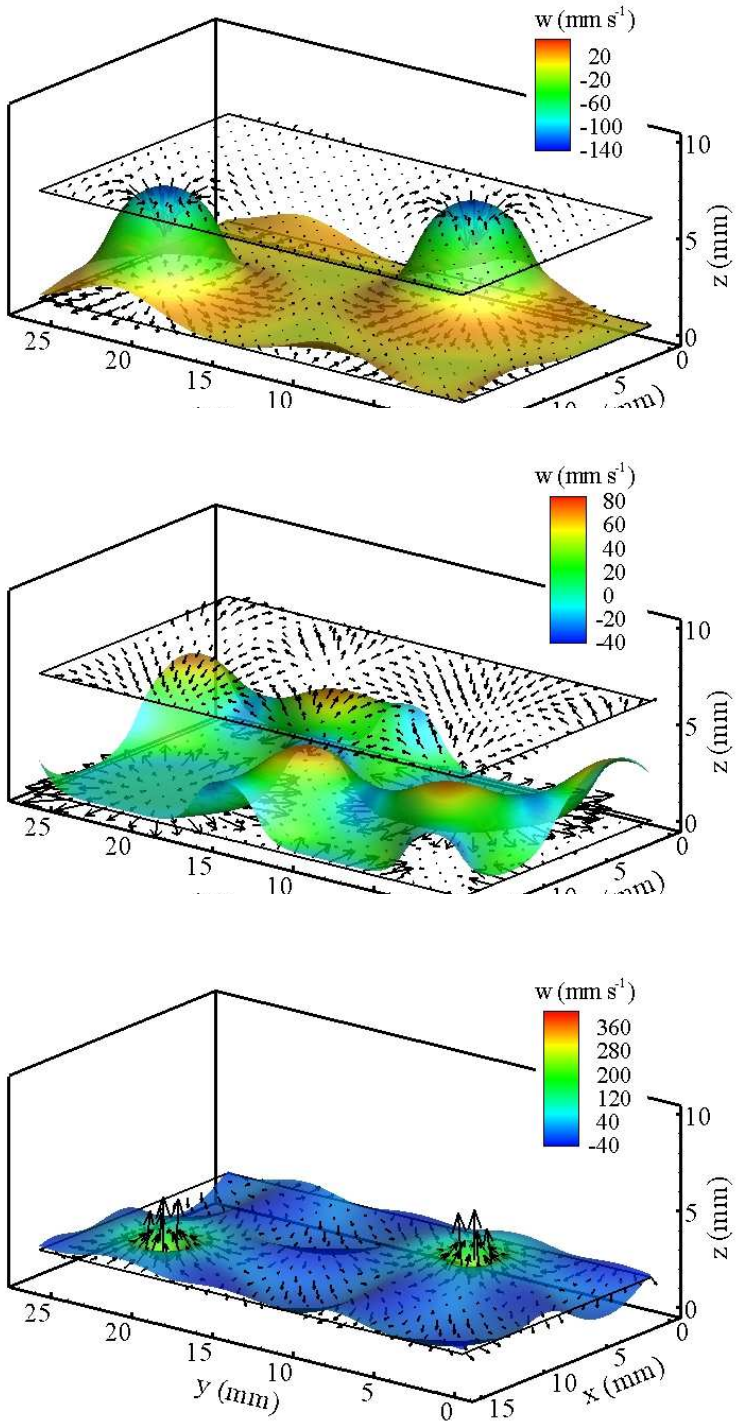

Hexagonal pattern in Faraday experiment

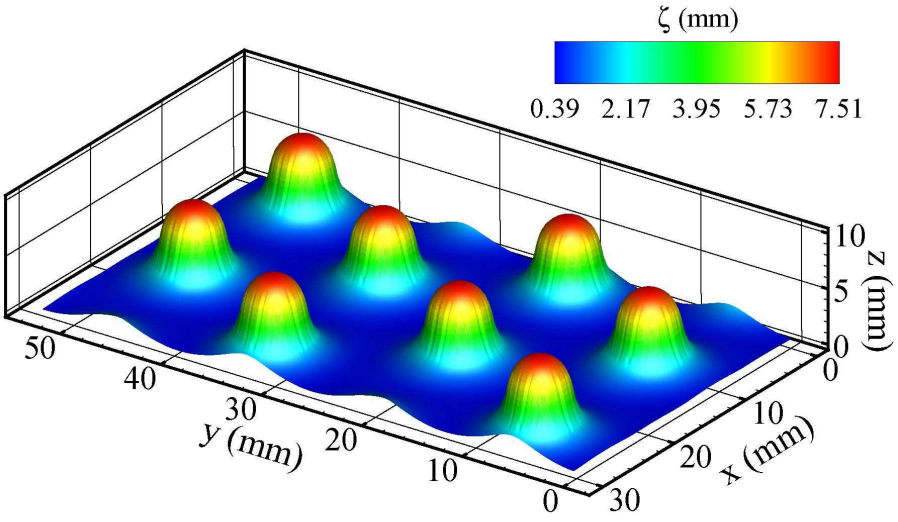

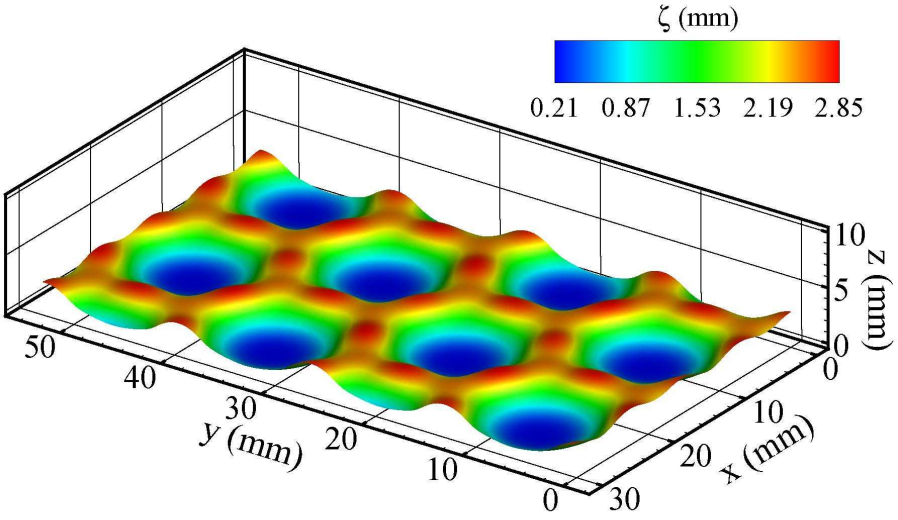

Hexagonal pattern in Faraday experiment

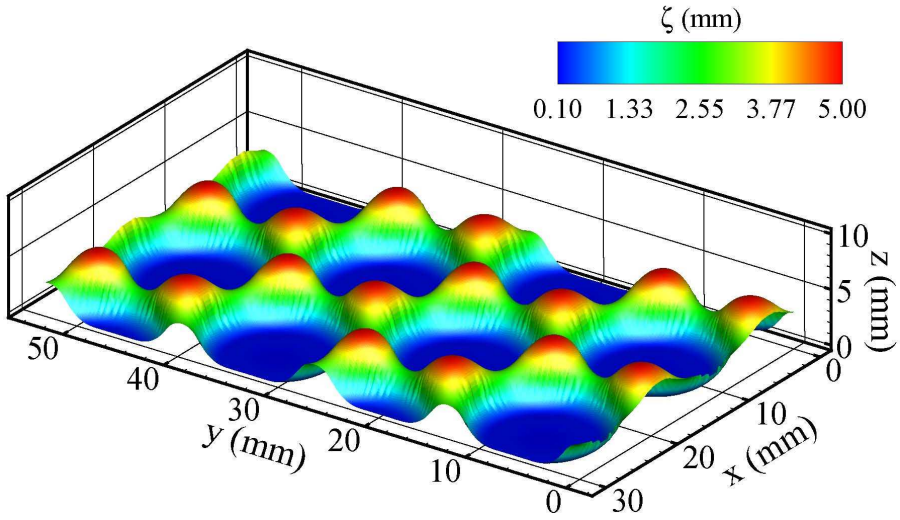

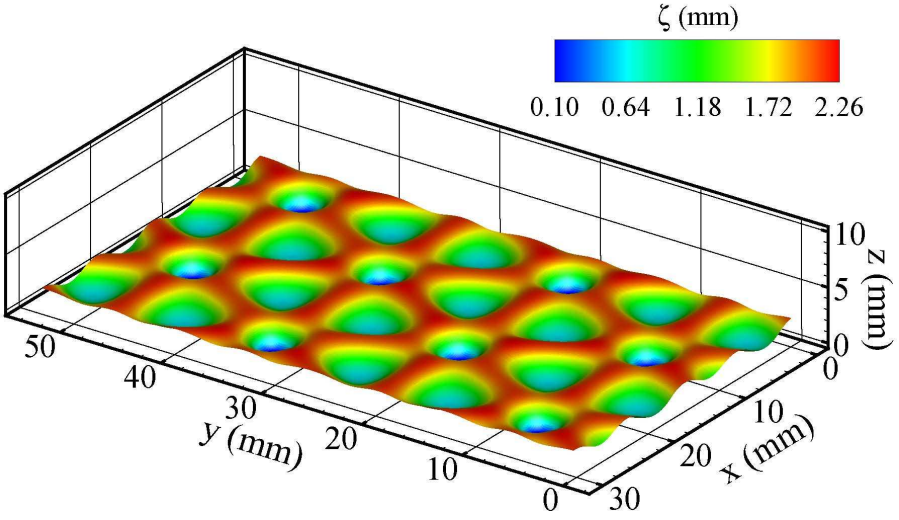

2 Instabilities of roll patterns

The Swift-Hohenberg equation reproduces many of the well-known instabilities of striped (roll) patterns:
– the **Eckhaus (E) instability**: change in wavelength
– the **zigzag (Z) instability**: sinusoidal in-phase oscillations along roll axes
– the **skew-varicose (SV) instability**: sinusoidal out-of-phase oscillations along roll axes
– the **cross-roll (CR) instability**: appearance of perpendicular rolls
– the **oscillatory (OS) instability**: time-dependent oscillations along roll axes

These were discovered numerically and explored extensively in a series of papers by Friedrich Busse and R. Clever in the 1970s on Rayleigh-Bénard convection. The occurrence of these instabilities depends on three parameters: Rayleigh number Ra, Prandtl number Pr and wavenumber α (also denoted by k) of the underlying striped (roll) pattern. The volume in (wavenumber, Rayleigh, Prandtl) space within which straight roll patterns are stable to these instabilities is called the **Busse balloon**, shown in figure 15

The fact that these patterns and instabilities also occur in the Swift-Hohenberg equation shows that they are not particular to Rayleigh-Bénard convection. Figures 16 and 17 shows the manifestation of some of these in experiments and simulations of a granular layer subjected to vertical oscillation, together with an adaptation of the Busse balloon to this case; the amplitude Γ of the vibrations acts analogously to the Rayleigh number.

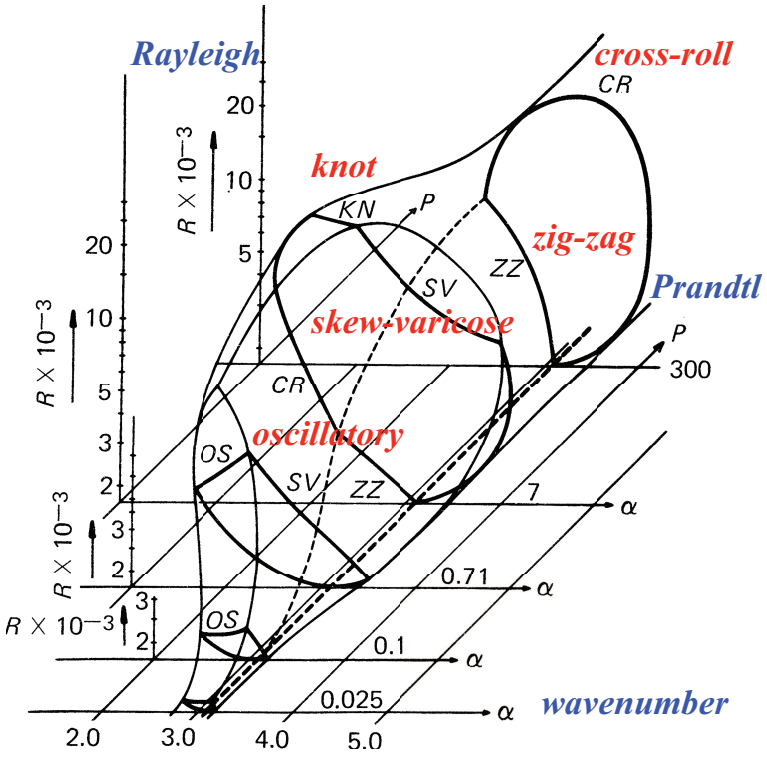

Figure 15: Busse balloon. Region in (wavenumber, Rayleigh, Prandtl) parameter space in which straight rolls are stable is delimited by various instabilities. From F.H. Busse, Transition to turbulence in Rayleigh-Bénard convection, in Hydrodynamic Instabilities and the Transition to Turbulence, ed. by H.L. Swinney and J.P. Gollub, Springer, 1981.

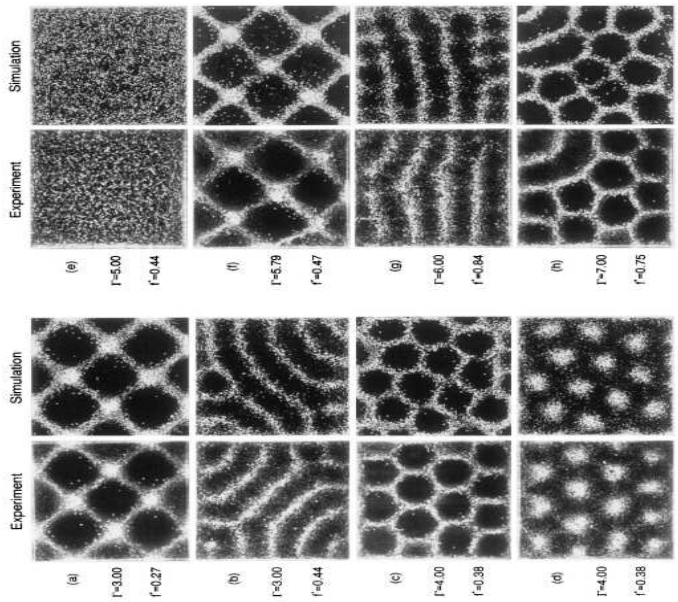

Figure 16: Squares, stripes, hexagons in a granular layer. From C. Bizon, M.D. Shattuck, J.B. Swift, W.D. McCormick & H.L. Swinney, *Patterns in 3D vertically oscillated granular layers: simulation and experiment*, Phys. Rev. Lett. **80**, 57 (1998).

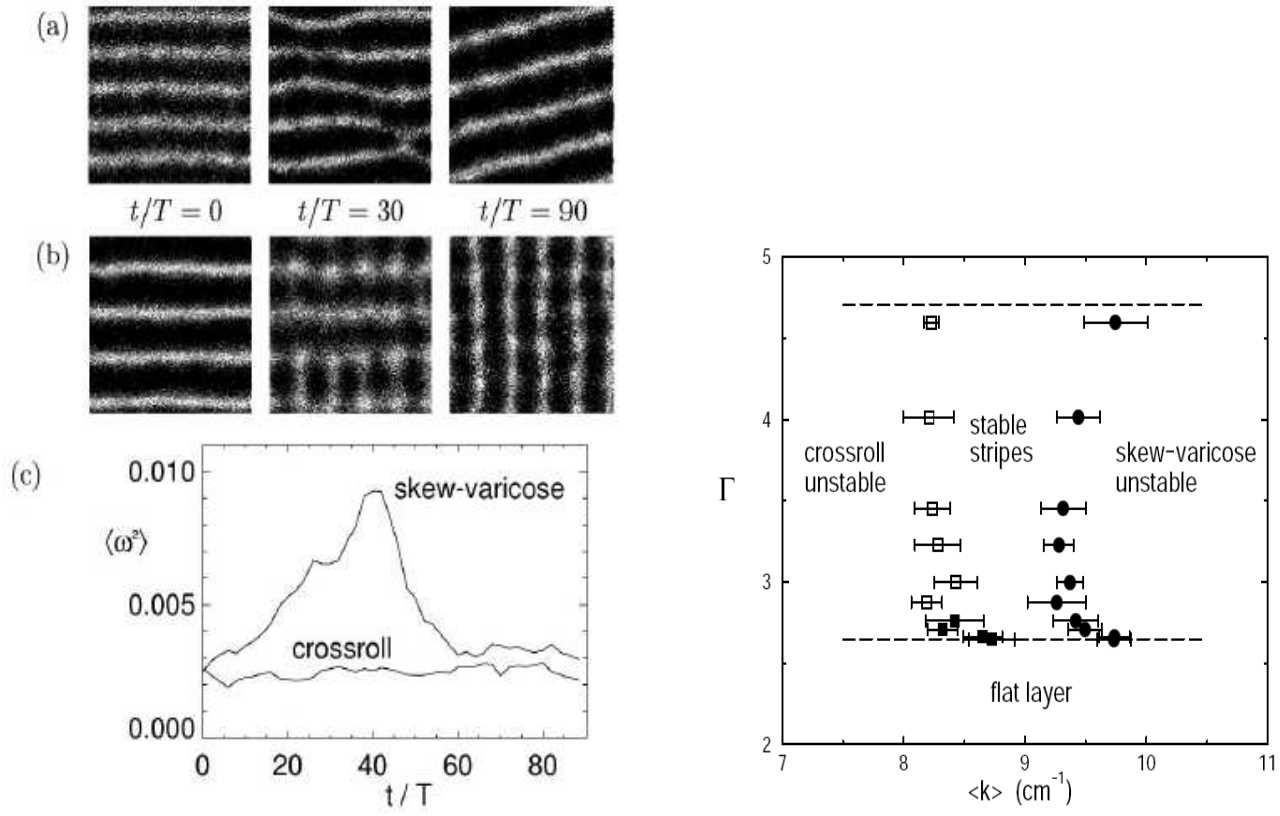

Figure 17: Instabilities of a striped pattern in a vertically-vibrated granular layer. Left top: skew-varicose instability. Left bottom: cross-roll instability. Right: stability boundaries in the $(< k >, \Gamma)$ plane, where $< k >$ is the mean wavenumber and Γ is the amplitude of the acceleration. From J. de. Bruyn, C. Bizon, M.D. Shattuck, D. Goldman, J.B. Swift & H.L. Swinney, *Continuum-type stability balloon in oscillated granulated layers*, Phys. Rev. Lett. **81**, 1421 (1998).

2.1 Newell-Whitehead-Segur equation

We will now investigate the stability of a pattern of rolls with wavenumber not too far from the critical wavenumber q_c. An amplitude A is defined, which depends on space and time via slow variables X, Y, T.

$$u(x, y, t) = A(X, Y, T)e^{iq_c x} + c.c. \tag{27}$$

The method of multiple scales is then used to derive from the Swift-Hohenberg equation for u an amplitude or envelope equation for A, formulated in 1969 by Newell, Whitehead and Segur:

$$\partial_T A = \mu A - |A|^2 A + \left(\partial_X - \frac{i}{2}\partial_{YY}\right)^2 A \tag{28}$$

For notational simplicity, we will revert to using x, y, t instead of X, Y, T.

$$\partial_t A = \mu A - |A|^2 A + \left(\partial_x - \frac{i}{2}\partial_{yy}\right)^2 A \tag{29}$$

The uniform state A=constant corresponds to a pattern of rolls with wavenumber q_c and oriented in the x direction. A pattern of rolls with a wavelength $q_c + q$ (where $q > -q_c$) is described by $A_q \sim e^{iqx}$, which bifurcates from $A = 0$ at $\mu = q^2$ and satisfies:

$$0 = \mu - |A_q|^2 - q^2 \Longrightarrow A_q = \sqrt{\mu - q^2}e^{i\phi}e^{iqx} \tag{30}$$

We linearize (29) about A_q by substituting $A_q + e^{\sigma t}a(x, y)$ into (29) and neglecting nonlinear terms:

$$\sigma a = \mu a - 2|A_q|^2 a - A_q^2 a^* + \left(\partial_x - \frac{i}{2}\partial_{yy}\right)^2 a \tag{31}$$

2.2 Eckhaus instability

We begin by considering only variation in x. Such eigenvectors of (31) are of the form:

$$\begin{aligned} a_0(x) &\equiv \alpha_0 e^{iqx} && \text{(32a)} \\ a_k(x) &\equiv \alpha_k e^{i(q+k)x} + \beta_k e^{i(q-k)x}, \quad k > 0 && \text{(32b)} \end{aligned}$$

Using

$$\begin{aligned} \left(\mu - 2|A_q|^2 + \partial_{xx}\right) a_0 &= (\mu - 2(\mu - q^2) - q^2)\alpha_0 e^{iqx} = -(\mu - q^2)\alpha_0 e^{iqx} && \text{(33a)} \\ A_q^2 a_0^* &= (\mu - q^2)e^{i2qx}\alpha_0^* e^{-iqx} = (\mu - q^2)\alpha_0^* e^{iqx} && \text{(33b)} \end{aligned}$$

we find

$$\sigma a_0 = -(\mu - q^2)\alpha_0 e^{iqx} - (\mu - q^2)\alpha_0^* e^{iqx} \tag{34}$$

or

$$\sigma_0 \begin{pmatrix} \alpha_0^R \\ \alpha_0^I \end{pmatrix} = \begin{pmatrix} -2(\mu - q^2) & 0 \\ 0 & 0 \end{pmatrix} \begin{pmatrix} \alpha_0^R \\ \alpha_0^I \end{pmatrix} \tag{35}$$

The eigenvalues along the diagonal are the usual eigenmodes of a circle pitchfork, corresponding to contraction with rate $\sigma_{0-} = -2(\mu - q^2)$ onto the circle of solutions and to the marginal stability ($\sigma_{0+} = 0$) along the circle. For $k > 0$, we use

$$\begin{aligned} (\mu - \ 2|A_q|^2 \ + \partial_{xx})a_k & \\ &= \left(\mu - 2(\mu - q^2) - (q+k)^2\right)\alpha_k e^{i(q+k)x} + \left(\mu - 2(\mu - q^2) - (q-k)^2\right)\beta_k e^{i(q-k)x} \\ &= -\left(\mu - q^2 + k^2 + 2qk\right)\alpha_k e^{i(q+k)x} - \left(\mu - q^2 + k^2 - 2qk)\right)\beta_k e^{i(q-k)x} \qquad \text{(36)} \\ A_q^2 a_k^* \quad = \quad & (\mu - q^2)e^{i2qx}\left(\alpha_k^* e^{-i(q+k)x} + \beta_k^* e^{-i(q-k)x}\right) = (\mu - q^2)\left(\alpha_k^* e^{i(q-k)x} + \beta_k^* e^{i(q+k)x}\right) \end{aligned}$$

so that

$$\begin{aligned} \sigma_k a_k &= -\left(\mu - q^2 + k^2 + 2qk\right)\alpha_k e^{i(q+k)x} - \left(\mu - q^2 + k^2 - 2qk\right)\beta_k e^{i(q-k)x} \\ &\quad -(\mu - q^2)\left(\alpha_k^* e^{i(q-k)x} + \beta_k^* e^{i(q+k)x}\right) \end{aligned}$$

which is expressed in matrix form as:

$$\sigma_k \begin{pmatrix} \alpha_k^R \\ \beta_k^R \end{pmatrix} = \begin{pmatrix} -(\mu - q^2 + k^2) - 2qk & -(\mu - q^2) \\ -(\mu - q^2) & -(\mu - q^2 + k^2) + 2qk \end{pmatrix} \begin{pmatrix} \alpha_k^R \\ \beta_k^R \end{pmatrix} \tag{37}$$

and a similar system for (α_k^I, β_k^I), with the off-diagonal terms of opposite sign from (37). Eigenvalues of

$$\begin{pmatrix} a - c & b \\ b & a + c \end{pmatrix} \tag{38}$$

are

$$\sigma = \frac{(a-c) + (a+c)}{2} \pm \sqrt{\left(\frac{(a-c) - (a+c)}{2}\right)^2 + b^2} = a \pm \sqrt{c^2 + b^2} \tag{39}$$

The systems for (α_k^R, β_k^R) and (α_k^I, β_k^I) lead to the same eigenvalues (which are therefore double):

$$\sigma_{k\pm} = -(\mu - q^2 + k^2) \pm \sqrt{(2qk)^2 + (\mu - q^2)^2} \tag{40}$$

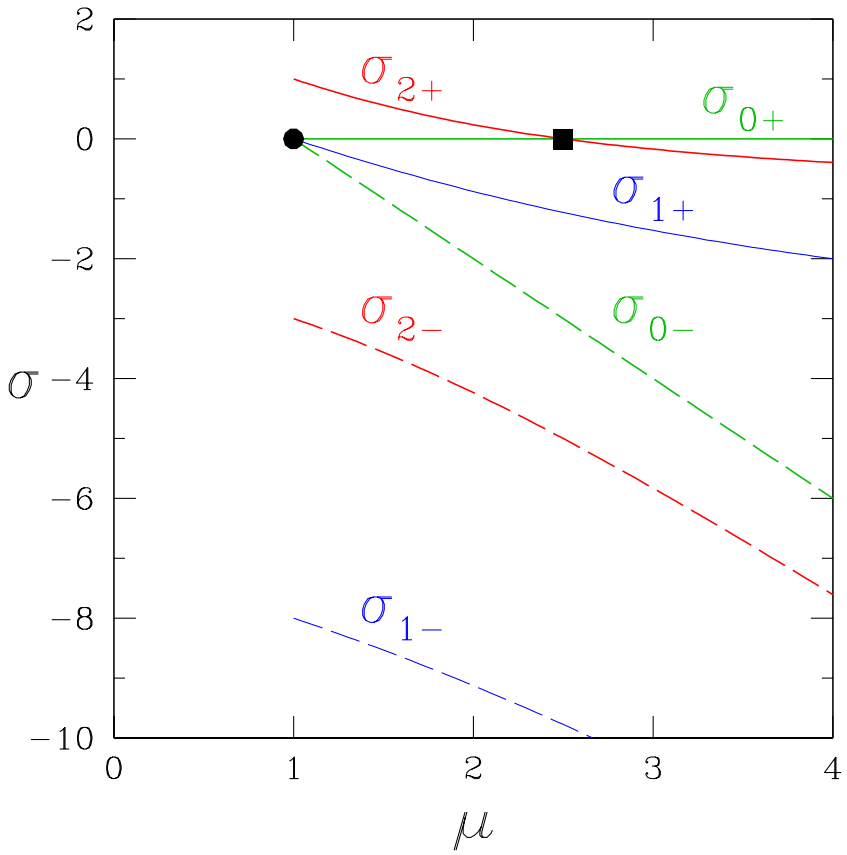

Figure 18: Eigenvalues $\sigma_{k\pm}$ of A_q for $q = 1$, $k = 0$, 1, 2. Branch A_q is created from the trivial state at a primary circle pitchfork bifurcation (●) and stabilized at a secondary Eckhaus bifurcation (■).

These eigenvalues are shown in figure 18. We call the corresponding eigenvectors $a_{k\pm}$.

Eigenvalues σ_{k-} and $\sigma_{0\pm}$ are always negative. At the bifurcation point $\mu = q^2$ at which A_q is created

$$\sigma_{k+} = -k^2 + |2qk| = k(2|q| - k) \tag{41}$$

and hence is positive if $k < 2|q|$. This means that, when it is created, branch A_q is unstable to the eigenvectors a_{k+} for $k < 2|q|$. The greater the value of q, i.e. the deviation from the critical wavenumber, the more unstable directions, since there are more possible values of k which satisfy this criterion. The eigenvalues associated with these unstable eigenvectors cross zero at:

$$\begin{aligned} (\mu - q^2 + k^2)^2 &= (2qk)^2 + (\mu - q^2)^2 \\ k^4 + 2(\mu - q^2)k^2 &= (2qk)^2 \\ (\mu - q^2) &= 2q^2 - \frac{k^2}{2} \\ \mu &= 3q^2 - \frac{k^2}{2} \end{aligned} \tag{42}$$

These points are shown in figure 19. Each of these points corresponds to a pitchfork bifurcation. Since these bifurcations occur from a branch already created via a bifurcation from the trivial state, they are

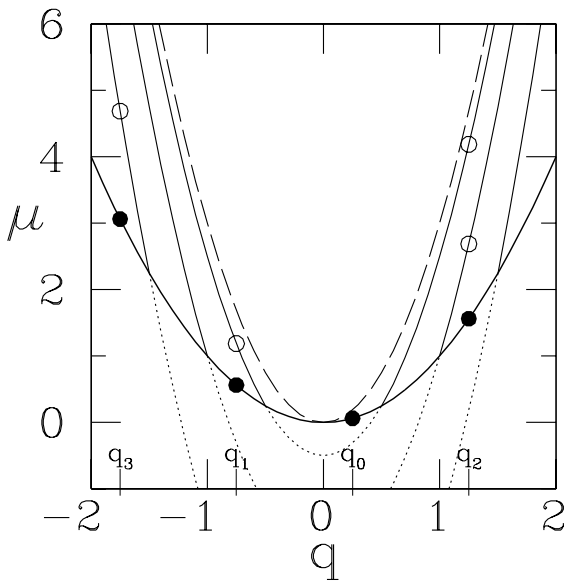

Figure 19: Stability curves. The thick parabola shows the marginal stability curve $\mu_q = q^2$ along which the trivial state is destabilized by primary bifurcations to periodic patterns A_q. Thin parabolas show the finite-domain Eckhaus curves $\mu_{qk} = 3q^2 - k^2/2$ for $k = 1, 2, \ldots$ along which the periodic patterns are stabilized by successive secondary bifurcations to unstable mixed-mode states. The highest of these, $\mu_{\text{finite}} = \mu_{q1} = 3q^2 - 1/2$, is the finite-domain Eckhaus boundary above which pattern A_q is stable. The dotted portions of the Eckhaus curves below the marginal stability curve have no significance, since states A_q do not exist in this region. Primary and secondary bifurcations for the specific case $q_c - [q_c] = -1/4$ are shown as solid and hollow dots, respectively. The infinite-domain Eckhaus curve $\mu_\infty = 3q^2$ is shown for contrast as a dashed curve.

called *secondary* bifurcations. New states emerge from these secondary bifurcation points, towards increasing μ, i.e. where A_q is more stable, and so the bifurcations are called *subcritical*. The bifurcation diagram is shown in figure 20.

When the last of these points is crossed, all of the eigenvalues have become negative and A_q is stable. This change of stability of A_q is the Eckhaus instability: We recall that q and k must be multiples of $2\pi/L$, with $q_n = 2n\pi/L$. The lowest value of μ in (42) is attained for $k = 2\pi/L$. Equation (42) takes on the more universal form

$$\mu_E = \left(3n^2 - \frac{1}{2}\right)\left(\frac{2\pi}{L}\right)^2 \Longleftrightarrow \hat{\mu}_E \equiv \left(\frac{L}{2\pi}\right)^2 \mu_E = 3n^2 - \frac{1}{2} \tag{43}$$

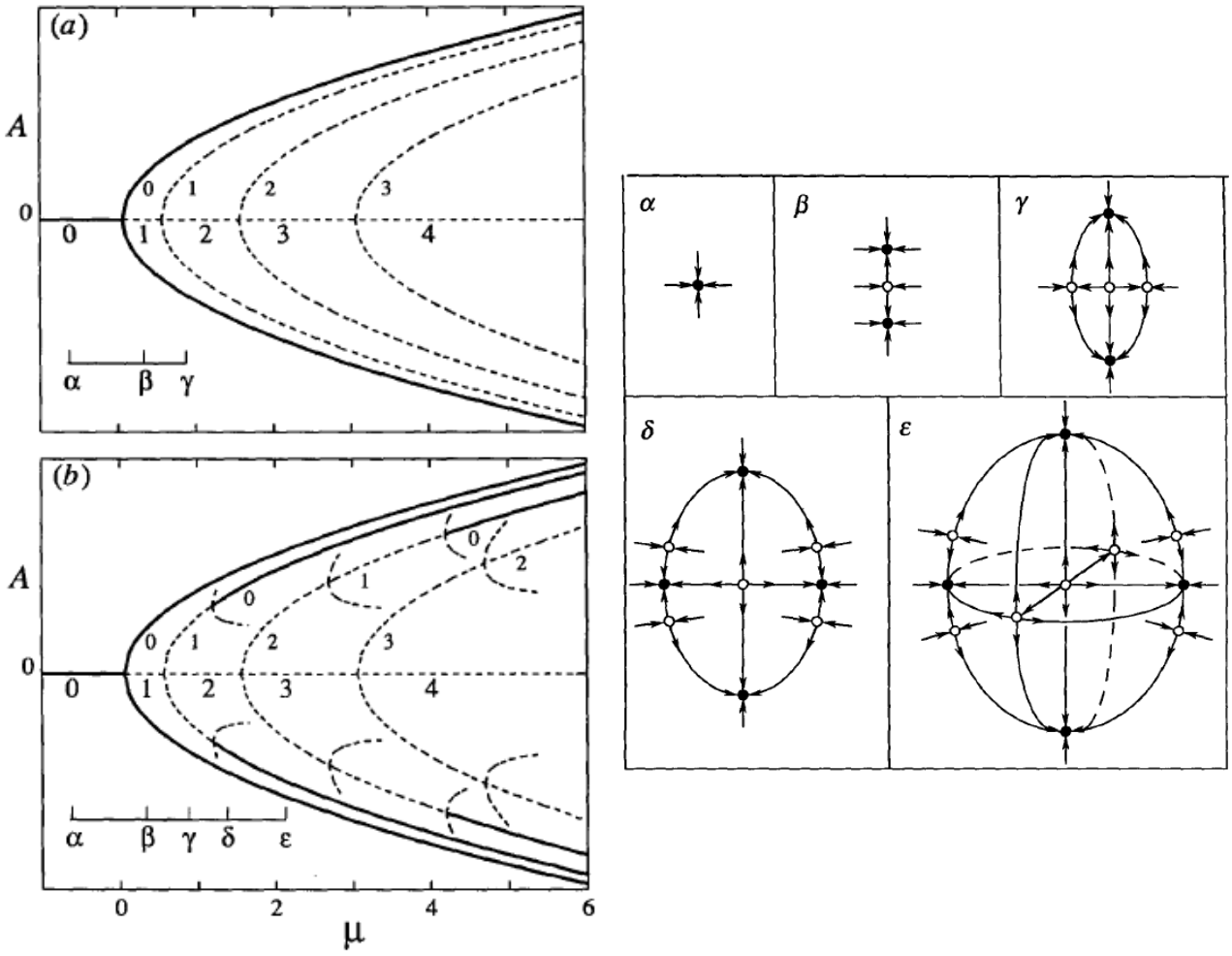

Figure 20: Left: bifurcation diagram. Branches with wavenumbers $q_0, q_1, q_2 \cdots$ are created at successive primary pitchfork bifurcations as μ is increased through the values $q_0^2, q_1^2, q_2^2, \cdots$. All but the first ($q_0$) branch is unstable; each branch is restabilized by successive secondary Eckhaus bifurcations at $\mu = 3q_n - k^2$. For clarity, only the lowest-μ portions of the mixed-mode branches created at the Eckhaus bifurcations are shown. Thick curves indicate stable portions of the trivial and primary branches. Right: schematic phase portraits at values of μ indicated on left. The coordinates represent projections of the first two or unstable directions of the trivial state C. Stable steady states are indicated by filled circles, unstable steady states by hollow circles. (α) For $\mu < 0$, C is the only steady state. C is stable as indicated by the solid circle and by the arrows pointing towards it. (β) After one supercritical bifurcation the trivial state is unstable and a pair of stable steady states A_0 (whose wavenumber is q_0, the allowed wavenumber closest to q_c) has been created. (γ) After a second supercritical bifurcation, C has two unstable directions. Another pair of steady states A_1, with allowed wavenumber q_1 now exists. These, however, are unstable (in one direction), as can be seen from the trajectories leading to A_0. These trajectories and unstable directions are inherited from C. (δ) States A_1 have been stabilized by undertoing a subcritical bifurcation. Each state A_1 emits a pair of unstable steady states, on the trajectories joining A_0 and A_1. (ϵ) C has undergone another supercritical bifurcation, acquiring a third unstable direction, and creating another pair of unstable steady states A_2. Each new state has two unstable directions, as can be seen from the trajectories joining A_2 to A_0 (towards the north and south poles) and to A_1 (left and right along the equator). States A_2 would require two subcritical bifurcations, one in each unstable direction, in order to become stable.

2.3 Zig-zag instability

We now carry out a similar analysis, but for variation in y. We seek eigenvectors of (31) of the form:

$$a_m(x) \equiv \alpha_m e^{i(qx+my)} + \beta_m e^{i(qx-my)}, \quad m > 0 \tag{44}$$

Using:

$$\begin{aligned}
\left(\partial_x - \frac{i}{2}\partial_{yy}\right)^2 e^{i(qx\pm my)} &= \left(iq - \frac{i}{2}(im)^2\right)^2 e^{i(qx\pm my)} = -\left(q + \frac{m^2}{2}\right)^2 e^{i(qx\pm my)} \\
&= -\left(q^2 + qm^2 + \frac{m^4}{4}\right) e^{i(qx\pm my)} \qquad (45) \\
(\mu - 2|A_q|^2)a_m &= (\mu - 2(\mu - q^2))a_m = (-\mu + 2q^2)a_m \qquad (46) \\
A_q^2 a_m^* &= (\mu - q^2)e^{i2qx}\left(\alpha_m^* e^{-i(qx+my)} + \beta_m^* e^{-i(qx-my)}\right) \\
&= (\mu - q^2)\left(\alpha_m^* e^{i(qx-my)} + \beta_m^* e^{i(qx+my)}\right) \qquad (47)
\end{aligned}$$

equation (31) becomes

$$\begin{aligned}
\sigma_m\left(\alpha_m e^{i(qx+my)} + \beta_m e^{i(qx-my)}\right) &= \left(-\mu + 2q^2 - q^2 - qm^2 - \frac{m^4}{4}\right)\left(\alpha_m e^{i(qx+my)} + \beta_m e^{i(qx-my)}\right) \\
&\quad -(\mu - q^2)\left(\alpha_m^* e^{i(qx-my)} + \beta_m^* e^{i(qx+my)}\right) \\
&= \left(-(\mu - q^2) - m^2\left(q + \frac{m^2}{4}\right)\right)\left(\alpha_m e^{i(qx+my)} + \beta_m e^{i(qx-my)}\right) \\
&\quad -(\mu - q^2)\left(\alpha_m^* e^{i(qx-my)} + \beta_m^* e^{i(qx+my)}\right) \qquad (48)
\end{aligned}$$

which is expressed in matrix form as:

$$\sigma_m \begin{pmatrix} \alpha_m^R \\ \beta_m^R \end{pmatrix} = \begin{pmatrix} -(\mu - q^2) - m^2\left(q + \frac{m^2}{4}\right) & -(\mu - q^2) \\ -(\mu - q^2) & -(\mu - q^2) - m^2\left(q + \frac{m^2}{4}\right) \end{pmatrix} \begin{pmatrix} \alpha_m^R \\ \beta_m^R \end{pmatrix} \tag{49}$$

Eigenvalues of

$$\begin{pmatrix} a & b \\ b & a \end{pmatrix} \tag{50}$$

are

$$\sigma = \frac{a+a}{2} \pm \sqrt{\left(\frac{(a-a)}{2}\right)^2 + b^2} = a \pm b \tag{51}$$

Hence the eigenvalues of (49) are

$$\sigma_m = -(\mu - q^2) - m^2\left(q + \frac{m^2}{4}\right) \pm (\mu - q^2) = \begin{cases} -m^2\left(q + \frac{m^2}{4}\right) \\ -2(\mu - q^2) - m^2\left(q + \frac{m^2}{4}\right) \end{cases} \tag{52}$$

For $q + \frac{m^2}{4} < 0$, i.e. for $q < -\frac{m^2}{4}$, the first eigenvalue above is positive, independent of μ. As for the Eckhaus case, the larger the value of $|q|$, the more unstable m modes there are. This instability occurs only for q negative, i.e. for wavenumbers smaller than – and wavelengths larger than – the critical values. As the rolls bend under the influence of the zig-zag instability, their wavelengths decrease.